Rock and Soil Mechanics

Volume 43 | Issue 3 Article 1

5-17-2022

Experimental study on the permeability characteristics of laminated shale under cyclic loading

Chuang ZHANG
College of Resources and Safety Sciences, Chongqing University, Chongqing 400044, China

Song REN
College of Resources and Safety Sciences, Chongqing University, Chongqing 400044, China, rs_rwx@163.com

Fei WU
College of Resources and Safety Sciences, Chongqing University, Chongqing 400044, China

Jie LIU
College of Resources and Safety Sciences, Chongqing University, Chongqing 400044, China

See next page for additional authors

Custom Citation

ZHANG Chuang, REN Song, WU Fei, LIU Jie, ZHOU Xu-hui, . Experimental study on the permeability characteristics of laminated shale under cyclic loading[J]. Rock and Soil Mechanics, 2022, 43(3): 649-658.

Experimental study on the permeability characteristics of laminated shale under cyclic loading

Authors

Chuang ZHANG, Song REN, Fei WU, Jie LIU, and Xu-hui ZHOU

Rock and Soil Mechanics 2022 43(3): 649−658 ISSN 1000−7598
https: //doi.org/10.16285/j.rsm.2021.5583 rocksoilmech.researchcommons.org/journal

Experimental study on the permeability characteristics of laminated shale under cyclic loading

ZHANG Chuang[1, 2], REN Song[1, 2], WU Fei[1, 2], LIU Jie[1, 2], ZHOU Xu-hui[1, 2]
1. State Key Laboratory of Coal Mine Disaster Dynamics and Control, Chongqing University, Chongqing 400044, China
2. College of Resources and Safety Sciences, Chongqing University, Chongqing 400044, China

Abstract: It is of great significance for the safe construction of shale gas tunnels to deeply understand the evolution law of permeability of laminated shale with macro fractures under cyclic disturbance. The permeability evolution of shale specimens containing axial beddings and axial macro fractures under cyclic axial stress and cyclic confining pressure was experimentally studied using the GCTS rock mechanics testing system. The results show that the permeability of shale specimens containing axial beddings did not change significantly during the loading and unloading of axial stress, but it decreased in a negatively exponential form with the increasing confining pressure and increased exponentially with the decreasing confining pressure. The permeability of shale samples containing macroscopic fractures decreased linearly with the increasing axial stress and increased linearly with the decreasing axial stress, while it decreased in a negatively exponential form with increasing confining pressure and increased exponentially with the increasing confining pressure. The permeability of shale specimens containing axial fractures is significantly higher than that of shale specimens with axial beddings, about 9 times the later one. The sensitivity of shale specimens to confining pressure is about 26 times that to axial stress. The permeability of the specimen almost keeps constant regardless of the number of axial stress loadings and unloadings, but decreases in a negatively exponential form with the increasing confining pressure cycles, and the major reduction occurs in the first cycle. The findings can somewhat provide theoretical support for the safe construction of shale gas tunnels.

Keywords: tunnel; shale; bedding; fracture; cyclic loading

1 Introduction

China is abundant in shale gas deposits and ranks among the top countries in the world[1−3]. 29.28% and 31.38% of the national recoverable shale gas reserves are in hilly and mountainous areas, respectively[4]. In addition, with the rapid development of infrastructure in China, shale gas tunnels are encountered frequently in the construction of road tunnels. Compared with coal strata, gas emissions in shale gas tunnels tend to be random and uncertain[5]. Therefore, accidents caused by gas emissions increace in the construction process of shale gas tunnels, causing massive mortality and property loss[6]. As the tunnel face is gradually advanced during the construction process, the surrounding rock ahead is in a cyclic loading stress state, and the number of cycles increases with the increasing distance to the tunnel face. Therefore, enhancing the experimental research on shale permeability characteristics under cyclic loadings is of great significance to deeply understand the shale gas migration in the surrounding rock, to accurately predict the gas emission amount from tunnels and to effectively avoid gas accidents.

Extensive research has been conducted on the permeability characteristics of shales and abundant meaningful results have been obtained. In terms of shale permeability mechanisms, Cui et al.[7] summarized the characterization techniques, classifications and evolution laws of shale pores. Zhang et al.[8] pointed out that the seepage channels in shale included micro-pores, micro-fractures, laminae and hydraulic fractures, and studied the seepage mechanisms of shale gas in channels with different scales. Chen et al.[9] found that the transport of shale gas in pores is mainly influenced by porosity, pore size, and pore connectivity. Sang et al.[10] stated that shale permeability is also affected by adsorption, desorption and slip. Wei et al.[11] also stated that the seepage process of shale gas mainly includes desorption, diffusion, slip, and Darcy flow. With respect to shale gas seepage models, Singh et al.[12] proposed a new model to characterize the permeability of shale gas by comprehensively considering of the pore size, gas pressure and isothermal adsorption. Gao et al.[13] established a nonlinear flow model for the apparent permeability of shale gas by taking the adsorption and desorption into account. Li et al.[14] developed a shale permeability model

Received: 17 April 2021 Revised: 17 December 2021
This work was supported by the National Natural Science Foundation of China (52074048, 51774057).
First author: ZHANG Chuang, male, born in 1987, PhD candidate, majoring in rock mechanics and engineering. E-mail: xfzhang@cqu.edu.cn
Corresponding author: REN Song, male, born in 1975, PhD, Professor, research interests: geotechnical engineering and reliability analysis. E-mail: rs_rwx@163.com

applicable to true triaxial stress anisotropy. Zhang et al.[15−17] indicated that shale reservoir permeability models mainly consists of three types: core permeability models, fractured core permeability models and fracture permeability models, and further conducted an in-depth study on fracture permeability models and the evolution law of shale gas reservoir permeability. Moreover, the relationship between shale permeability and stress has also been widely studied[18−22], and the results show that the variation of shale permeability is closely related to the stress magnitude. For example, shale permeability gradually decreases with the increasing effective stress. Chen et al.[23] conducted an experimental study on the permeability characteristics of laminated shales, and pointed out that the permeability characteristics of laminated shales have significant anisotropy and confining pressure sensitivity. Jiang et al.[24] examined the permeability characteristics of laminated shales under true triaxial conditions and found that the intermediate principal stress and lamina direction are the two main factors affecting the shale permeability characteristics. Peng et al.[25] investigated the permeability characteristics of rough fractures within shales and pointed out that the relationship between pressure gradient and flow rate is closely related to the confining pressure. At a low confining pressure, the relationship between them can be described by the Forchheimer equation. The fractures tend to close and the flow rate tends to stabilize under a high confining pressure. Ma et al.[26] explored the permeability characteristics of fractured shales and pointed out that its permeability exhibited a gradual decreasing tendency with increasing axial stress, whose specific relationship follows the logarithmic distribution.

In summary, the current research work on shale permeability characteristics mainly concentrates on the microstructure characterization, seepage path partition, seepage mechanism revelation, and permeability model establishment. Although some experimental studies on shale permeability characteristics were reported, most of them were conventional compression tests on homogeneous shales. However, the public literature on the seepage properties of shale specimens containing laminae or macroscopic fractures under cyclic loadings are very limited. Under construction disturbance, macroscopic fractures are often generated along the shale lamina direction since shales are typical sedimentary rocks with extensive internal laminae. Furthermore, due to the randomness of stratigraphic occurrence, the tunneling direction may be either parallel or perpendicular to the lamina direction. In view of this, shale specimens with the most unfavorable laminae angle (the axial direction) were chosen as the research objects to conduct experiments on the evolution of shale permeability under cyclic axial loads and cyclic confining pressures using GCTS rock mechanics test system. The findings can effectively guarantee the safe construction of shale gas tunnels.

2 Experiment overview

2.1 Specimen preparation

The specimens with developed laminae, belonging to Longmaxi Formation, were taken from the palm face of Mazui tunnel in Nanchuan, Chongqing. The rock blocks from the field were brought to the laboratory. The cores were drilled along the bedding direction and then processed into 50 mm×100 mm standard cylindrical specimens after being cut and polished, as shown in Fig.1. It can be seen from Fig.1 that the bedding development direction in the sample is parallel to the axial direction of the sample.

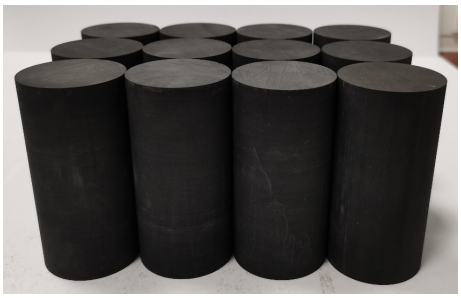

Fig. 1 Shale samples

2.2 Test apparatus

The tests were carried out using the GCTS rock mechanics test system at State Key Laboratory of Coal Mine Disaster Dynamics and Control, Chongqing University, as shown in Fig.2. The equipment can not only simulate the stress, pore pressure and temperature conditions of deep underground rocks, but also carry out uniaxial compression, indirect tension, triaxial compression, fatigue, creep, relaxation tests, and even measure the ultra-low permeability of rocks under high temperature and pressure. The specific parameters are as follows: the maximum axial force, the maximum confining pressure, the maximum gas pressure and the accuracy of gas pressure sensors are 2 800 kN, 80 MPa, 15 MPa and 0.01 MPa, respectively. In summary, the GCTS rock mechanics test system completely meet the requirements of the present experimental study.

2.3 Test programs

Half of the specimens (6) were taken to be split into

(a) Real equipment

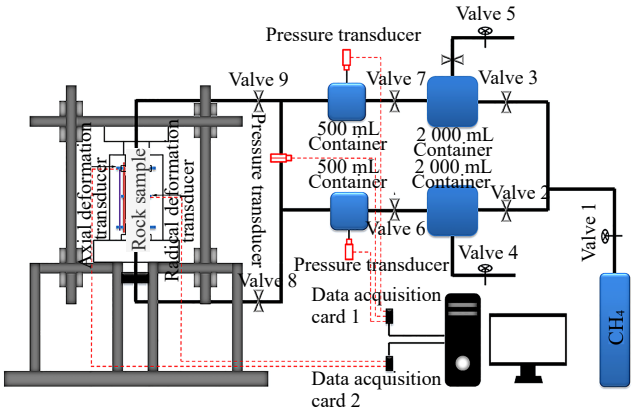

(b) Schematic diagram

Fig. 2 GCTS rock mechanics test system

two halves along the direction of lamina development, and the halves were then reassembled along the splitting surface. The reassembled specimens thus contained macroscopic fractures parallel to its axial direction.

The laminated shale specimens (6) and the specimens containing macroscopic fractures (6) were divided into two and numbered as I-1, I-2, I-3, II-1, II-2, II-3, III-1, III-2, III-3, and IV-1, IV-2, IV-3, respectively. The specimens of types I and III are used to conduct axial loading and unloading tests, while the specimens of types II and IV are used to conduct the confining pressure loading and unloading tests, whose stress path diagram is shown in Fig.3. In addition, the test information such as stress magnitude and number of cycles for each type of specimens is listed in Table 1.

In particular, according to geological conditions, the average density of Longmaxi Formation shales in the tunnel site area is approximately 2.6 g /cm^3, the tunnel burial depth is about 150 m, and the internal shale gas pressure in surrounding rocks is about 2.5 MPa. In view of this, the cyclic stress was set between 3 and 6 MPa. Additionally, given that the permeability of shale specimens containing macroscopic fractures is larger than that of laminated shale specimens, a larger stress is required to reduce the permeability to a relatively uniform level. Therefore, the cyclic stress was set as 5−10 MPa for fractured shale specimens.

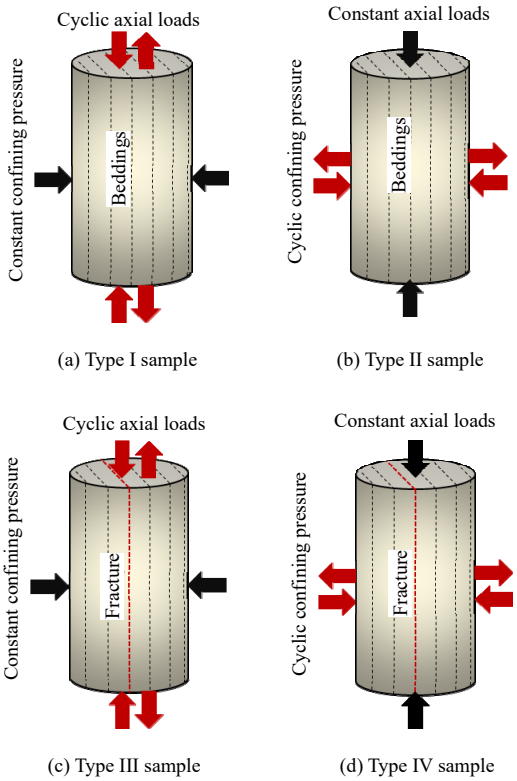

(a) Type I sample (b) Type II sample

(c) Type III sample (d) Type IV sample

Fig. 3 Loading path

Table 1 Test scheme

Specimen No.	Cyclic stress	Stress values	Cyclic number n	Gas pressure p /MPa
I-1 I-2 I-3	Axial stress	σ_1 is 3−6 MPa, σ_3 is 3 MPa	5	2.5
II-1 II-2 II-3	Confining stress	σ_1 is 3 MPa, σ_3 is 3−6 MPa	5	2.5
III-1 III-2 III-3	Axial stress	σ_1 is 5−10 MPa, σ_3 is 5 MPa	5	2.5
IV-1 IV-2 IV-3	Confining stress	σ_1 is 5 MPa, σ_3 is 5−10 MPa	5	2.5

Note: σ_1 and σ_3 are the axial stress and confining pressure, respectively.

2.4 Test procedures

The schematic diagram of the test device is shown in Fig.2(b). Taking the type I specimen as an example, the test steps are described in detail as follows:

(1) First, a layer of heat-shrinkable tubing was wrapped around the specimen, which was then placed in the loading chamber. The chamber should be sealed perfectly.

(2) Both the axial stress and confining pressures were loaded to 3 MPa at a loading rate of 0.05 MPa/s.

(3) The gas was gradually injected into the lower gas

storage chamber by opening valves 1, 2 and 6. These valves should not be closed until the gas pressure in the storage chamber reached 2.5 MPa.

(4) The gas gradually flew from the lower gas storage chamber to the upper gas storage chamber via the specimen by opening valves 8 and 9. During this process, the change of gas pressure versus time in the upper and lower gas storage chambers was recorded until the gas pressure in the upper and lower gas storage chambers was in a balance state.

(5) The stored gas was expelled from the chambers by opening valves 4, 5, 6 and 7. The axial stress was loaded to 6 MPa at a gradient of 0.5 MP, and then was unloaded at the same gradient. This process was repeated 5 times, and steps (3) and (4) at each stress level were also repeated in order to obtain the permeability of the specimen at a given stress level.

3 Test results and analysis

Since the permeability of shale specimens is small, the transient method is used herein to calculate the permeability by the following expression:

$$\left(p_{\mathrm{u}}-p_{\mathrm{f}}\right)=\Delta p_0\times\frac{v_{\mathrm{d}}}{v_{\mathrm{u}}+v_{\mathrm{d}}}\times\mathrm{e}^{-\alpha t} \tag{1}$$

$$\alpha=-\frac{kA}{\mu c_{\mathrm{f}}L}\times\left(\frac{1}{v_{\mathrm{u}}}+\frac{1}{v_{\mathrm{d}}}\right) \tag{2}$$

where k is the permeability (m^2); c_{f} is the gas compressibility coefficient (1/Pa); μ is the dynamic viscosity ($\mathrm{N\cdot s/m^2}$); L and A are the length (m) and area (m^2) of the specimen, respectively; v_{u} and v_{d} are the volume of the upper and lower gas storage chambers (m^3); p_{u} is the gas pressure pf the upper chamber (Pa); p_{f} is the final gas equilibrium pressure (Pa); Δp_0 is the initial differential pressure (Pa); t is time (s); and α is the slope of the semi-logarithmic decay curve.

To eliminate the errors caused by test dispersion, three specimens were used for each type of test, and the test results were analyzed by their average value.

3.1 Permeability evolution under each cyclic load

The permeability evolution law of shale specimens under each cyclic load is shown in Fig.4, where n is the number of cycles of the axial stress and confining pressure. It can be seen from the figure:

For shale specimens containing axial laminae under cyclic axial stress, the permeability nearly remained constant at 1.47×10^{-15} m^2 with the loading of axial stress. When the axial stress increased to a certain value, the permeability decreased slightly with the reduction of 0.08×10^{-15} m^2, accounting for approximately 5% of that before the stress was applied. The permeability regained the original value with the unloading of the axial stress. With the increase of axial stress cycles, the effective axial stress corresponding to the abrupt change in permeability gradually decreased, which was 4.25, 3.77, 3.77, 3.72, 3.29 MPa for the loading tests, and 4.26, 3.79, 3.29, 3.25, 3.24 MPa for the unloading process. From the above analysis, it can be concluded that the permeability of shale specimens containing axial laminae almost keeps fixed during the cyclic loading and unloading of axial stress (as shown in Fig.4(a)).

For shale specimens containing axial laminae under cyclic confining pressure, the permeability decreased in a negatively exponential form with increasing effective confining pressure during the loading process. During the unloading process of confining pressure, the permeability exponentially increased with the decreasing effective confining pressure. At a given cycle and a given effective confining pressure, the permeability under the loading path was significantly larger than that under the unloading path, and their difference increased with decreasing effective confining pressure. At a given effective confining pressure, the difference between the permeability under the loading path and under the unloading path decreased with increasing cycles. For example, with increasing cycles, the difference under the effective confining pressure of 1.75 MPa was 1.39×10^{-15}, 0.95×10^{-15}, 0.82×10^{-15}, 0.75×10^{-15} and 0.08×10^{-15} m^2 (as shown in Fig.4(b)). In addition, it can be seen from Fig.4(b) that with increasing cycles of the confining pressure, the average variation of permeability of the shale specimens containing axial laminae in the loading and unloading process of confining pressure was 1.16×10^{-15}, 0.88×10^{-15}, 0.79×10^{-15}, 0.76×10^{-15} and 0.76×10^{-15} m^2. By comparing Figs. 4(a) and 4(b), it can be seen that for the shale specimens containing axial laminae, the permeability variation under cyclic confining pressure is markedly larger than that under cyclic axial stress, i.e., the variation tendency of permeability versus effective stress is obviously anisotropic.

For shale specimens containing axial macroscopic fractures under cyclic axial stress, the permeability linearly decreased with increasing effective axial stress during the loading process, and it increased linearly with decreasing effective axial stress during the unloading process. Under the same effective axial stress, the permeability gradually increased with increasing cycles. For example, under the effective axial stress of 8.75 MPa, the permeability at different cycles was 12.35×10^{-15}, 12.48×10^{-15}, $12.54\times$

10^{-15}, 12.60×10^{-15} and 12.60×10^{-15} m^2, (as shown in Fig.4(c)). In addition, it can be seen from Fig.4(c) that with increasing cycles of axial stress, the average changing magnitude of the permeability of shale specimens containing axial macrofractures during the loading and unloading process was 0.41×10^{-15}, 0.22×10^{-15}, 0.22×10^{-15}, 0.19×10^{-15} and 0.19×10^{-15} m^2. Combined with Figs. 4(a) and 4(c), it can be concluded that under the cyclic axial stress, the permeability variation of shale specimens containing axial macrofractures is more significant than that of shale specimens containing axial lamina.

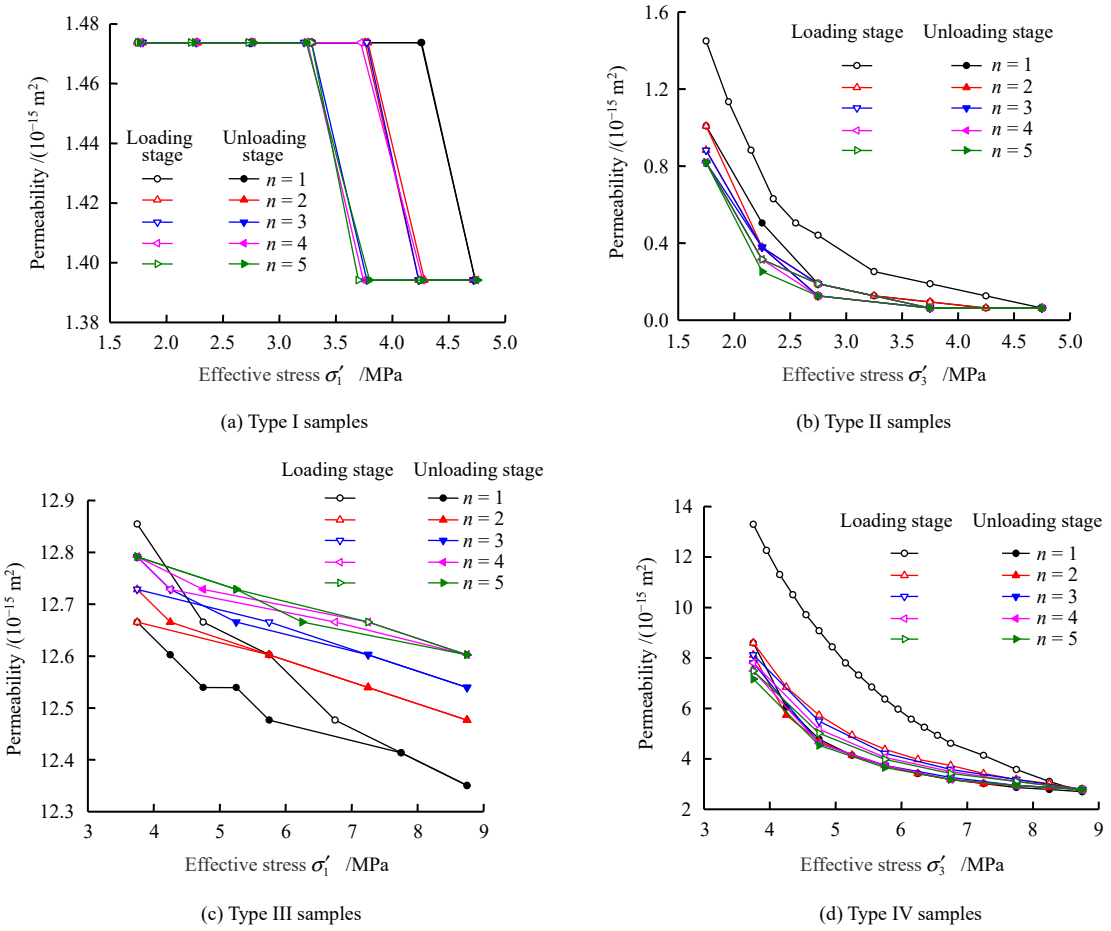

(a) Type I samples

(b) Type II samples

(c) Type III samples

(d) Type IV samples

Fig. 4 Relationships between permeability and stress under each loading and unloading round

For shale specimens containing axial macroscopic fractures under cyclic confining pressure, the variation of permeability with cyclic confining pressure is nearly consist with that of shale specimens containing axial laminae with cyclic confining pressure. They both decreased in a negatively exponential form with increasing confining pressure and increased exponentially with increasing confining pressure. For a given confining pressure, the permeability in the loading process was significantly larger than that under the unloading process, and the difference between them increased with the decreasing confining pressure and decreased with the increasing cycles. The difference was that the variation of the permeability of the shale specimens containing axial macrofractures with the confining pressure was more drastic than that of the specimens containing axial lamina with the confining pressure. The average variation magnitude of the permeability of the specimens containing axial lamina with different cyclic confining pressures was 8.24×10^{-15}, 5.57×10^{-15}, 5.17×10^{-15}, 4.85×10^{-15}, and 4.54×10^{-15} m^2 respectively (as shown in Fig.4(d)). In addition, comparison between Figs. 4(c) and 4(b) shows that the change in the permeability of shale specimens containing axial macrofractures under cyclic axial stress is more significant than the that of shale specimens containing axial macrofractures under cyclic confining pressure, i.e., the change in the permeability of shale specimens containing axial macrofractures with effective stress is also significantly anisotropic.

In summary, the evolution law of permeability of shale specimens with the effective stress is influenced by the internal structure type (axial laminae or axial

macroscopic fractures), the loading direction (cyclic axial stress or cyclic confining pressure), and the number of cycles.

3.2 Response of permeability to internal structures of specimens

Engineering disturbances are actually common and lead to different degrees of damage in the rock mass. Enhancing the study of the effect of internal structures on the permeability of shale specimens is of great significance for deep understanding the seepage characteristics of shale gas in rock masses.

Table 2 comparatively lists the permeability of shale specimens containing axial laminae before and after failure. It can be observed that the permeability of shale specimens with axial laminae and shale specimens with axial macroscopic fractures before cyclic loading was 1.47×10^{-15} and 13.02×10^{-15} m^2, respectively. After failure, the permeability of shale specimens was 8.86 times that before loading. After five cyclic loadings of axial stress, the permeability of shale specimens with axial lamina was 1.47×10^{-15} m^2, nearly unchanged compared with that before the loading of cyclic axial stress; while the permeability of shale specimens with axial macrofracture was 12.79×10^{-15} m^2, with a reduction of 0.65×10^{-15} m^2 and 8.70 times that before the loading of cyclic axial stress. After five cyclic loadings of confining stress, the permeability of shale specimens with axial lamina was 0.82×10^{-15} m^2, with a reduction of 0.23×10^{-15} m^2 compared with that before the loading of cyclic confining stress; while the permeability of shale specimens with axial macrofracture was 7.48×10^{-15} m^2, with a reduction of 5.54×10^{-15} m^2 and 9.12 times that before the loading of cyclic confining stress. From the above analysis, it can be seen that the permeability of shale specimens after failure increased significantly compared with that before loading, and the ratio of permeability of shale specimens before and after failure is affected by the cyclic loading, i.e., the ratio is negatively correlated with cyclic axial stress, while positively correlated with cyclic confining pressure.

Table 2 Comparison of the permeability before and after failure(unit: m^2)

Samples	Before cyclic loads	After 5 cyclic axial loads	After 5 cyclic confining pressure
Before failure	1.47×10^{-15}	1.47×10^{-15}	0.82×10^{-15}
After failure	13.02×10^{-15}	12.79×10^{-15}	7.48×10^{-15}

Therefore, to enhance the construction safety of shale gas tunnels, the gas emission should be reduced as much as possible. Specifically, minimize the damage extent of the excavated surrounding rock mass and provide strong support measures for the broken surrounding rock mass as early as possible

3.3 Response of permeability to load direction

In engineering projects, the lamina development inside the rock mass is often random, while the external construction disturbance is always directional. It is of great practical significance to strengthen the study on the effect of the angle between the load and lamina on shale permeability.

Define the sensitivity coefficient C_{k} of the permeability of shale specimens to stress as

$$C_{\mathrm{k}}=\frac{1}{k_{n0}}\frac{\Delta k_n}{\Delta p_n} \tag{3}$$

where k_{n0} is the permeability of the specimen before the n-th cycle; Δk_n is the change in permeability after the n-th loading; and Δp_n is the change in stress after the n-th loading.

The sensitivity coefficients of permeability to stress under different test conditions are listed in Table 3. It can be seen from Table 3 that before failure, the average value of the sensitivity coefficient of permeability to axial stress within 5 cycles of axial stress was 0.018, and counterpart to confining pressure was 0.311, about 17 times the former value. After failure, the average value of the sensitivity coefficient of permeability to axial stress within 5 cycles of axial stress was 0.004, and counterpart to confining pressure was 0.136, approximately 34 times the former value. From the above analysis, it can be inferred that the sensitivity of permeability to the confining pressure is much greater than that to the axial stress.

Table 3 Sensitivity coefficient of the shale permeability to stress

Cycle number	Axial loading and unloading		Loading and unloading of confining pressure	
	Before failure	After failure	Before failure	After failure
1	0.018	0.008	0.319	0.159
2	0.018	0.003	0.313	0.135
3	0.018	0.003	0.310	0.131
4	0.018	0.003	0.308	0.129
5	0.018	0.003	0.308	0.126

Note: The average values of the sensitivity coefficients before and after the failure of the specimen under the axial loading/unloading and confining pressure loading/unloading are 0.018, 0.004, 0.311 and 0.136, respectively.

Therefore, during the construction of shale gas tunnels,

to maximally reduce the permeability of the rock mass and thus guarantee a safe construction environment, it is necessary to ensure the construction direction perpendicular to the inner laminae of the shale as much as possible, in addition to minimizing the loosening circle of the tunnel surrounding rock.

3.4 Response of shale permeability to load cycles

In addition, since most of the loads on engineering rock masses are cyclic loads, it is also of great engineering significance to enhance the study of the variation law of shale permeability with the load cycles.

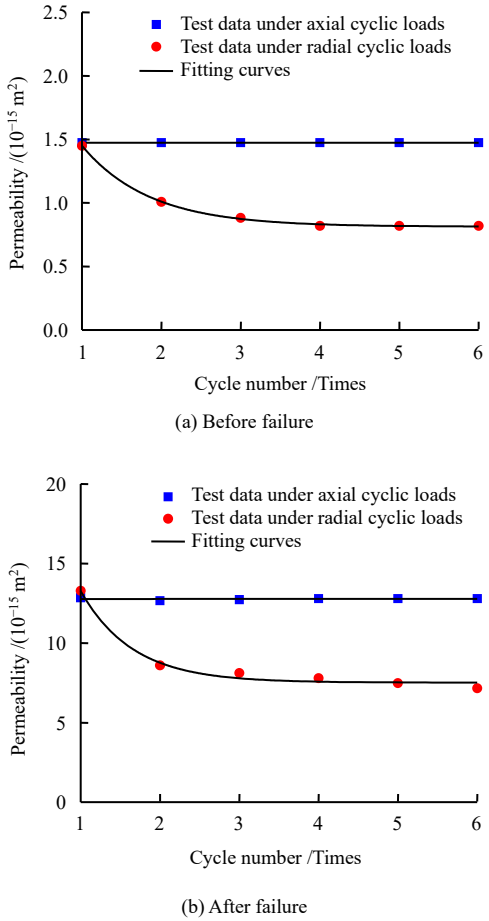

Fig. 5 Fitting curves of the relationship between permeability and cycle numbers

The variation law of shale permeability with the load cycles is shown in Fig.5. As can be seen from the figure, the permeability of shale specimens containing axial laminae was 1.47×10^{-15} m^2 before cyclic loading, and it remained constant with increasing the axial load cycles. When the specimens were subjected to cyclic confining pressure, the permeability decreased with increasing the load cycles, with the values of 1.01×10^{-15}, 0.88×10^{-15}, 0.82×10^{-15}, 0.82×10^{-15}, 0.82×10^{-15} m^2. For shale specimens containing axial fractures, the permeability before cyclic loading was 13.29 m^2, which remained constant with increasing the load cycles under cyclic axial stress. Once the specimens were under cyclic confining pressure, the permeability decreased with increasing the load cycles, with the values of 8.60×10^{-15}, 8.12×10^{-15}, 7.80×10^{-15}, 7.42×10^{-15}, 7.16×10^{-15} m^2. It can be seen that the permeability of both specimens containing axial laminae and specimens containing axial fractures decreases with increasing load cycles. The only difference is that the reduction in permeability of the specimens under cyclic confining pressure was greater than that under cyclic axial stress. Before failure, permeability gradually decreased with increasing the confining pressure cycles, and remained stable after 3 cycles. Notably, the reduction was larger at 69.84% in the first cycle. Similarly, after failure, the permeability decreased with increasing the confining pressure cycles, and remained stable after 5 cycles. Notably, the reduction was larger at nearly 80.72% in the first cycle.

As can be seen from the above, regardless of the failure of the specimens containing axial laminae, the permeability decreases with increasing the confining pressure cycles, and the reduction is the largest in the first cycle. The permeability tends to stabilize after a certain number of cycles.

The test results in Fig.5 can be fitted to obtain the permeability function to describe its relation with the confining pressure cycle, as listed in Table 4. It can be seen from Table 4 that the relation of permeability versus load cycles obeys the following exponential function:

$$k = a - b\times c^n \tag{4}$$

where k is the permeability of the specimen; a, b and c are the parameters related to the specimen.

Eq. (4) is a function between the permeability and the confining pressure cycles. The derivation of Eq. (4) shows that:

$$k' = -b\ln c\times c^n \tag{5}$$

Therefore, the parameter $-b\ln c\times c^n$ can somewhat represent the changing magnitude of permeability in response to the load cycles. Combined with Table 4, it can be seen that in the first cycle, i.e., n = 1, $-b\ln c\times c^n$ was 0.75 before failure and 8.80 after failure, indicating the permeability reduction after failure is significantly larger than the counterpart before failure during the first cycle. Similarly, the above law does not change significantly with the change of cycles under a given cycle number.

In addition, it is also seen from Eq. (4) that, since $0 < c < 1$, when $n \to \infty$, $k \to a$, the value of a represents the final value of permeability of the specimen after multiple cycles of loading. Combined with Table 4, it can be inferred that the permeability of the specimens before and after failure finally stabilizes approximately 0.812×10^{-15} m^2 and 7.516×10^{-15} m^2 after multiple confining pressure cycles.

Table 4 Fitting functions between permeability and cycle numbers under cyclic confining pressure

Samples	Fitting curves	Correlation R^2
Before failure	$k = 0.812 + 2.05\times0.312^n$	$R^2 = 0.999$
After failure	$k = 7.516 + 26.54\times0.217^n$	$R^2 = 0.980$

Therefore, frequently enhancing the support stress to the surrounding rocks can help reduce the amount of gas emission in an excavated tunnel, and the first round of support stress performs best.

4 Mechanism analysis

Figure 6 shows the CT scans of the shale specimen sections, where Fig.6(a) shows the electron microscope scan at the vertical laminae surface before failure. It can be seen that there are directionally distributed laminae development inside the shale specimen. Figure 6(b) illustrates the electron microscope scan profile parallel to the fracture surface after the failure of the specimen, which shows that numerous developed micropores and microfractures are randomly distributed in the shale specimen.

To obtain the scale distribution of microdefects (such as micropores, microfractures, laminae and macrofractures) inside the specimen, NMR tests were conducted on the shale specimens before and after failure. The pore size distribution characteristics were acquired based on the T_2 distribution diagram, as shown in Fig.7, where r is the pore size (μm). It can be seen from the figure that there are mainly three types of micro-defects inside the specimen before failure: micropores, microfractures and laminae, and the pore size of micropores and microfractures is at a same level, i.e., between 0.001 and 0.1 μm with the average value of 0.01 μm. The pore size of lamina is mainly between 0.32 and 3.16 μm with the average value of 1 μm. After failure, apart from the original defects such as micropores, microcracks and laminae, a new type of defects i.e., macrocracks, is generated. The pore size distribution range and the average value of micropores, microcracks and laminae inside the specimen change significantly after failure compared with those before failure. The distribution range of the pore size of macro-fractures is mainly between 5.02 and 31.62 μm with the average value of about 10 μm.

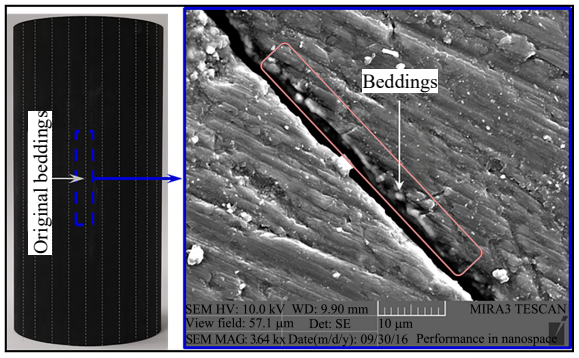

(a) Bedding structure

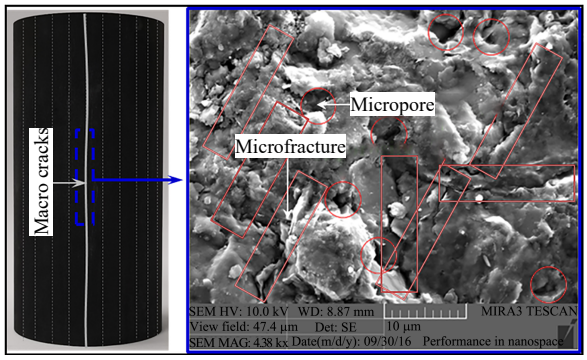

(b) Micropore/microfracture structure

Fig. 6 SEM images of specimen slices

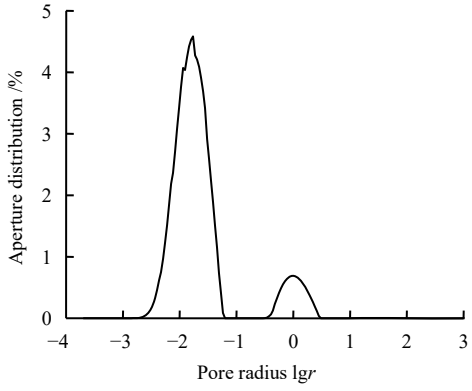

(a) Shale specimens containing axial beddings

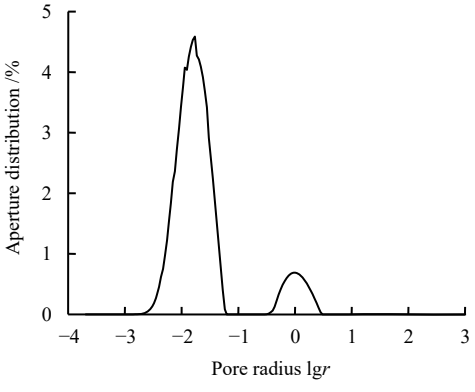

(b) Shale specimens containing axial fractures

Fig. 7 Sample aperture profiles

In summary, before the failure of the shale specimens, the internal seepage channels include micropores, microfractures and laminae, while macrofractures are added after failure. The pore size varies in order of magnitude between micropores/microfractures, laminae and macrofractures. The laminae and macrofractures inside the specimen are directionally distributed along the axial direction of the specimen.

From the above analysis, it can be concluded that the dominant factor of the shale permeability before failure is the laminae, while the macrofractures dominate the permeability after failure. The laminae and macrofractures have the same effect on the permeability variation, proportional to the opening size. Compared with the laminae, the aperture of macroscopic fractures increases by orders of magnitude, and therefore, thus resulting in a significant increase of the permeability after failure. In addition, for both laminae and macroscopic fractures, the main contributing factor for their opening sizes is the "engaging" effect of the rock on both sides of the structural face, which is related to the roughness of the structural surface, the stress along the normal direction of the structural surface, the load cycles, etc. The laminae and macroscopic cracks are distributed in the axial direction inside the specimen, indicating that the confining pressure affects the structural surface aperture by directly acting on the laminae or macrofractures, while the axial stress affects the structural surface opening indirectly through the Poisson effect. Hence, the permeability is more sensitive to confining pressure than axial stress. The surface of macrofractures is rougher than that of the laminae. The specimens after failure is thus more sensitive to the confining pressure. As the confining pressure cycles increase, the "engaging effect" between the laminae and macrofractures gradually maximizes. Consequently, the sensitivity of permeability to the confining pressure gradually decreases with increasing of cycles, and finally the permeability gradually tends to reach a constant value.

In summary, for shale specimens containing axial laminae, the main internal seepage channels are laminae, and the external stress mainly affects the permeability by altering the laminae aperture, which is determined by the engaging degree of the structural surfaces. Similarly, for shale specimens containing axial macrofractures, the internal seepage channels are mainly macrofractures, and the external stress mainly affects the permeability by altering the macrofracture aperture, which is also determined by the engaging degree of the structural surfaces.

5 Conclusions

Based on the study of permeability variation law of axially laminated and axially fractured shale specimens under cyclic axial loading and cyclic confining pressure, the following conclusions can be obtained:

(1) For shale specimens containing axial laminae, the permeability keeps unchanged with the cyclic loading and unloading of axial stress, and it decreases in a negatively exponential form with increasing confining pressure during the cyclic loading and unloading process of confining pressure. For shale specimens containing axial fractures, the permeability decreases linearly with the loading of axial stress and increases the linearly with the unloading of axial stress, and it decreases in a negatively exponential form with increasing the confining pressure and increases exponentially with decreasing the confining pressure during the cyclic loading and unloading process of confining pressure.

(2) The permeability of shale specimens containing axial fractures is significantly enhanced than that of shale specimens containing axial laminae. Before cyclic loading, the permeability of shale specimens containing axial fractures is 8.86 times that of shale specimens containing axial laminae. After 5 cycles of loading and unloading of axial stress, the permeability of shale specimens containing axial fractures is 8.70 times that of shale specimens containing axial laminae. After 5 cycles of loading and unloading of confining pressure, the permeability of shale specimens containing axial fractures is 8.70 times that of shale specimens containing axial laminae.

(3) For shale specimens containing axial laminae and shale specimens containing axial fractures, the permeability is more sensitive to the surrounding rock than the axial stress. The sensitivity coefficients of shale specimens containing axial laminae to the confining pressure and axial stress is 0.311 and 0.018 respectively with a ratio of 17.28. The sensitivity coefficients of shale specimens containing axial fractures to the axial stress and confining pressure is 0.004 and 0. 136 respectively with a ratio of 34.

(4) Under a cyclic axial stress, the permeability is unchanged with the increasing of load cycles. Under a cyclic confining pressure, the permeability decreases in a negatively exponential form with the increasing of load cycles. The major reduction of permeability with cyclic confining pressure occurs in the first cycle, where the reduction is about 69.84% and 80.72% for specimens before and after failure, respectively.

(5) Based on the above findings, for the construction

safety of shale gas tunnels, the gas emission can be effectively reduced by reducing the loosening circle of the surrounding rock, excavating in the direction perpendicular to the laminae, and improving the supporting frequency of the excavated surrounding rock mass.

References

[1] LI Jian-zhong, DONG Da-zhong, CHEN Geng-sheng, et al. Shale gas resource prospect and strategic position in China[J]. Geology and Exploration, 2009, 29(5): 11−16.

[2] DONG Da-zhong, WANG Yu-man, LI Xin-jing, et al. New breakthroughs and development prospects of shale gas exploration and development in China[J]. Natural Gas Industry, 2016, 36(1): 19−32.

[3] CHENG Yong, CHEN Guo-dong, YIN Qiong, et al. Shale gas exploration and development in China and its implications for North America[J]. Journal of Kunming Metallurgical College, 2017, 33(1): 16−24.

[4] LONG Sheng-xiang, CAO Yan, ZHU Jie, et al. Shale gas development prospect and related problems in China[J]. Oil & Gas Geology, 2016, 37(6): 847−853.

[5] ZHANG Chuang. Study on gas emission law and control measures in shale section of highway tunnel[D]. Chongqing: Chongqing University, 2018.

[6] KANG Xiao-bing. Study on gas hazard evaluation system of tunnel engineering[D]. Chengdu: Chengdu University of Technology, 2009.

[7] CUI Jing-wei, ZOU Cai-neng, ZHU Ru-kai, et al. New advances in shale porosity research[J]. Advances in Earth Science, 2012, 27(12): 1319−1325.

[8] ZHANG J, SCHERER G W. Permeability of shale by the beam-bending method[J]. International Journal of Rock Mechanics and Mining Sciences, 2012, 53: 179−191.

[9] CHEN S, HAN Y, FU C, et al. Micro and nano-size pores of clay minerals in shale reservoirs: implication for the accumulation of shale gas[J]. Sedimentary Geology, 2016, 342: 180−190.

[10] SANG G, ELSWORTH D, MIAO X, et al. Numerical study of a stress dependent triple porosity model for shale gas reservoirs accommodating gas diffusion in kerogen[J]. Journal of Natural Gas Science and Engineering, 2016, 32: 423−438.

[11] WEI Ming-qiang, DUAN Yong-gang, FANG Quan-tang, et al. Current research situation of porosity & permeability characteristics and seepage mechanism of shale gas reservoir[J]. Reservoir Evaluation and Development, 2011, 1(4): 73−77.

[12] SINGH H, JAVADPOUR F. Langmuir slip-Langmuir sorption permeability model of shale[J]. Fuel, 2016, 164: 28−37.

[13] GAO J, YU Q, LU X. Apparent permeability and gas flow behavior in carboniferous shale from the Qaidam Basin, China: an experimental study[J]. Transport in Porous Media, 2016, 116(2): 585−611.

[14] LI M, YIN G, XU J, et al. Permeability evolution of shale under anisotropic true triaxial stress conditions[J]. International Journal of Coal Geology, 2016, 165: 142−148.

[15] ZHANG Hong-xue, LIU Wei-qun. Relevant experiments, models and environmental effect of shale gas production[J]. Rock and Soil Mechanics, 2014, 35(Suppl.2): 85−100.

[16] ZHANG Hong-xue, LIU Wei-qun, ZHU Li. Fracture permeability model and experiments of shale gas reservoirs[J]. Rock and Soil Mechanics, 2015, 36(3): 719−729.

[17] ZHANG Hong-xue, LIU Wei-qun. Permeability evolution mechanism of shale gas reservoir under non-equilibrium desorption state[J]. Rock and Soil Mechanics, 2021, 42(10): 2696−2704.

[18] WANG Ji-lin, LIU Gui-jian, WANG Wei-zhong, et al. Characteristics of pore-fissure and permeability of shales in the Longmaxi formation in Southeastern Sichuan Basin[J]. Journal of China Coal Society, 2013, 38(5): 772−777.

[19] KWON O, KRONENBERG A K, GANGI A F, et al. Permeability of illite-bearing shale: 1. anisotropy and effects of clay content and loading[J]. Journal of Geophysical Research: Solid Earth, 2004, 109(B10): jb003052.

[20] NING Y, HE S, CHEN T, et al. Simulation of shale gas transport in 3D complex nanoscale-pore structures using the lattice Boltzmann method[J]. SPE Asia Pacific Unconventional Resources Conference and Exhibition, 2015: http://doi:10.2118/176997-ms.

[21] HELLER R, VERMYLEN J, ZOBACK M. Experimental investigation of matrix permeability of gas shales[J]. AAPG Bulletin, 2014, 98(5): 975−995.

[22] SONG W, YAO J, LI Y, et al. Apparent gas permeability in an organic-rich shale reservoir[J]. Fuel, 2016, 181: 973−984.

[23] CHEN Tian-yu, FENG Xia-ting, YANG Cheng-xiang, et al. Research on confining pressure sensitivity and anisotropy for gas shale permeability[J]. Journal of Mining & Safety Engineering, 2014, 31(4): 639−643.

[24] JIANG Chang-bao, CHEN Yu-fei, YIN Guang-zhi, et al. Experimental study on the effect of intermediate principal stress and bedding direction on mechanical properties and permeability of shale[J]. Chinese Journal of Rock Mechanics and Engineering, 2017, 36(7): 1570−1578.

[25] PENG Hui-hua, ZHOU Lei, LU Yi-yu. Experimental study on conductivity of rough shale fractures using methane[J]. Chinese Journal of Rock Mechanics and Engineering, 2016, 35(Suppl.2): 3644−3652.

[26] MA Zhan-guo, MIAO Xie-xing, LI Xing-hua, et al. Permeability of broken shale[J]. Journal of Mining & Safety Engineering, 2007, 24(3): 260−264.